Matrix Biology Plus 23 (2024) 100151

Contents lists available at ScienceDirect

Matrix Biology Plus

journal homepage: www.sciencedirect.com/journal/matrix-biology-plus

Engineering a robust and anisotropic cardiac-specific extracellular matrix scaffold for cardiac patch tissue engineering

Te-An Chen [a], Brandon B. Zhao [a], Richard A. Balbin [a], Sameeksha Sharma [a], Donggi Ha [b], Timothy J. Kamp [c,d], Yuxiao Zhou [b], Feng Zhao [a,*]

[a] Department of Biomedical Engineering, Texas A&M University, College Station, TX 77843, USA
[b] Department of Mechanical Engineering, Texas A&M University, College Station, TX 77843, USA
[c] Department of Medicine, University of Wisconsin-Madison, Madison, WI 53705, USA
[d] Stem Cell and Regenerative Medicine Center, University of Wisconsin-Madison, Madison, WI 53705, USA

ARTICLE INFO

Keywords:
Extracellular matrix
Cardiac tissue engineering
Cardiac patch scaffold
Cardiac fibroblasts
Micropattern

ABSTRACT

Extracellular matrix (ECM) fabricated using human induced pluripotent stem cells (hiPSCs)-derived cardiac fibroblasts (hiPSC-CFs) could serve as a completely biological scaffold for an engineered cardiac patch, leveraging the unlimited source and outstanding reproducibility of hiPSC-CFs. Additionally, hiPSC-CF-derived ECM (hiPSC-CF-ECM) holds the potential to enhance maturation of exogenous cardiomyocytes, such as hiPSC-derived cardiomyocytes (hiPSC-CMs), by providing a microenvironment rich in cardiac-specific biochemical and signaling cues. However, achieving sufficient robustness of hiPSC-CF-ECM is challenging. This study aims to achieve appropriate ECM deposition, scaffold thickness, and mechanical strength of an aligned hiPSC-CF-ECM by optimizing the culture period, ranging from 2 to 10 weeks, of hiPSC-CFs grown on micro-grated substrates, which can direct the alignment of both hiPSC-CFs and their secreted ECM. The hiPSC-CFs demonstrated a production rate of 13.5 μg ECM per day per 20,000 cells seeded. An anisotropic nanofibrous hiPSC-CF-ECM scaffold with a thickness of 20.0 ± 2.1 μm was achieved after 6 weeks of culture, followed by decellularization. Compositional analysis through liquid chromatography-mass spectrometry (LC-MS) revealed the presence of cardiac-specific fibrillar collagens, non-fibrillar collagens, and matricellular proteins. Uniaxial tensile stretching of the hiPSC-CF-ECM scaffold indicated robust tensile resilience. Finally, hiPSCs-CMs cultured on the hiPSC-CF-ECM exhibited alignment following the guidance of ECM nanofibers and demonstrated mature organization of key structural proteins. The culture duration of the anisotropic hiPSC-CF-ECM was successfully refined to achieve a robust scaffold containing structural proteins that resembles cardiac microenvironment. This completely biological, anisotropic, and cardiac-specific ECM holds great potential for cardiac patch engineering.

Introduction

Tissue engineering strategies for the reconstruction of injured tissues involve the use of implantable scaffolds [1], which not only serve as a structural framework for cells but also facilitate efficient transport of soluble gases and nutrients, ensuring the survival of infiltrated cells and their integration with host tissue [2,3]. Decellularized extracellular matrix (ECM), a biomaterial scaffold generated from mammalian cell sheets, tissues, or organs through the removal of immunogenic cellular components via decellularized technologies, stands out as one of the most studied scaffold materials widely applied to soft tissues and organs reconstruction [4–6]. Specifically, as a delivery vehicle for exogenous cardiomyocytes, such as human induced pluripotent stem cells (hiPSCs)-derived cardiomyocytes (hiPSC-CMs), natural ECM minimizes cell loss and yields a better clinical outcome compared to conventional injection-based therapies [7,8]. Moreover, in contrast with fibrin-based hydrogels that have been previously used to engineer cardiac patches [9–12], natural ECM comprises comprehensive bioactive molecules and biochemical factors inherent in native tissues. However, decellularized natural ECM obtained from allogenic or xenogeneic tissues faces challenges related to the scarcity of autologous tissue/organs, and the risk of pathogen transfer [13]. On the other hand, ECM scaffold derived from human cells can undergo pathogen screening to secure a pathogen-free environment [5]. Therefore, human cell-derived ECM represents a more

* Corresponding author.
E-mail address: fengzhao@tamu.edu (F. Zhao).

https://doi.org/10.1016/j.mbplus.2024.100151
Received 15 March 2024; Received in revised form 22 April 2024; Accepted 18 May 2024
Available online 25 May 2024

promising alternative to ECM derived from natural tissues, ensuring a safer and more reproducible microenvironment.

Native cardiac ECM is a complex meshwork of fibrillar and non-fibrillar components that not only provide structural support but also regulate the fate of cardiomyocytes, endothelial cells, and smooth muscle cells, dictating their differentiation, migration, proliferation, and overall homeostasis [14,15]. Two essential compartments are comprised in the native cardiac ECM: interstitial matrix and basement membrane. Interstitial matrix is primarily composed of collagen I and III, which offers structural and mechanical support. In contrast, basement membrane consists mainly of fibronectin, laminin, pro-collagens, hyaluronic acid, and proteoglycans. These components play a role in regulating the polarity, differentiation, and migration of cardiac cells through signals received on their cell surfaces [14]. This complex network also serves as a reservoir of ECM-bound growth factors, cytokines, matrix metalloproteinases (MMPs), chemokines, protease inhibitors, and noncoding RNAs [14–16]. Within the native heart, cardiac fibroblasts are the main contributor for ECM production and growth factor secretion [15]. By harnessing the *in vitro* secretion of ECM from cardiac fibroblasts cell sheets, we can generate a diverse array of protein fractions within this cell-derived ECM. Moreover, current hiPSC technologies offer an unlimited source of genetically identical cardiac fibroblasts due to the sustained renewal of hiPSCs in culture [17]. This makes hiPSC-derived cardiac fibroblasts (hiPSC-CFs) not only an unlimited source, but also an excellent candidate for the fabrication of cell-derived ECM.

The objective of this study was to generate a robust scaffold containing structural proteins that resemble cardiac microenvironment for cardiac patch engineering. We have previously generated an anisotropic and cardiac-specific ECM scaffold from a hiPSC-CF sheet grown on micro-grated pattern, following by decellularization [18]. The aligned hiPSC-CF cell sheet-derived ECM (hiPSC-CF-ECM) scaffold not only contains biomacromolecules and growth factors that are specific to the native cardiac microenvironment but also provides an anisotropic template for cellular alignment. However, short-term cell culture duration, which is typically up to several days, cannot provide a sufficient robustness of cell-secreted ECM for cardiac patch engineering. On the other side, while an extended culture period facilitates cell proliferation and ECM secretion, a potential challenge arises from the diffusion issue, leading to cell death. This study aims to optimize the fabrication of hiPSC-CF-ECM by refining the culture conditions to reach applicable ECM deposition, scaffold thickness and mechanical strength. hiPSC-CFs were cultured over an extended culture period for up to 10 weeks on micropatterned polydimethylsiloxane (PDMS) substrates. Optimal culture duration was determined through morphological analysis, thickness measurement, and DNA concentration of cell sheets and decellularized ECM, followed by characterization of composition and mechanical properties highlighting the diverse components and durability of the optimal hiPSC-CF-ECM. Finally, the effectiveness of hiPSC-CF-ECM in supporting the functional maturation of hiPSC-CMs was evaluated by examining the expression of specific structural protein and the contractility of cardiomyocytes grown on the ECM scaffold. Overall, the current work delineates an optimal fabrication process to generate an aligned cardiac-specific ECM scaffold for cardiac patch engineering.

Materials and methods

hiPSC-CF differentiation

hiPSCs (DF19-9-11T, WiCell Research Institute Inc., Madison, WI, USA) cultured with StemFlex media (Thermo Scientific, Waltham, MA, USA) were dissociated using Versene solution (Gibco, Thermo Scientific, Waltham, MA, USA) and incubated 37 °C for 5 min. Subsequently, cells were seeded onto 6-well plate coated with Matrigel (GFR, Corning Inc., Corning, NY, USA) at a density of 200,000 cells/cm^2 in mTeSR1 medium (STEMCELL Technologies, Vancouver, BC, Canada) supplemented with 10 μM ROCK inhibitor (Y-27632, Tocris, Bristol, UK). The medium was changed every day for 5 days until they reached confluency (day 0). On day 0, medium was switched to RPMI/B27-insulin media (B27 Supplement minus insulin, Gibco) with an addition of 12 μM CHIR99021 (Tocris) for 24 h. Following this, the medium was changed to fresh RPMI/B27-insulin for the next 42 h. After 66 h (day 2.75) of CHIR99021 treatment, the medium was replaced with CFBM [17] supplemented with 75 ng/ml bFGF (WiCell Research Institute). The medium was changed every other day until day 20. Then, cells were collected for flow cytometry analysis to assess the purity of the differentiated hiPSC-CFs. Pure hiPSC-CFs (>70 % TE7$^+$) were then cryopreserved.

hiPSC-CM differentiation

hiPSC-CM was differentiated followed by the GiWi protocol [19]. Briefly, hiPSCs (DF19-9–11 T, WiCell Research Institute) were seeded onto 6-well plate coated with Matrigel (GFR, Corning) at a density of 200,000 cells/cm^2 in mTeSR1 medium (STEMCELL Technologies) with 10 μM ROCK inhibitor (Y-27632, Tocris). The medium was changed every day until reaching confluency (day 0). On day 0, medium was changed to RPMI/B27-insulin media (B27 Supplement minus insulin, Gibco) supplemented with 12 μM CHIR99021 (Tocris) for 24 h. Followed by 24 h (day 1), the medium was changed to fresh RPMI/B27-insulin for 48 h until day 3. On day 3, cells were treated with 5 μM IWP2 (Tocris) in a blend of medium (half of the old medium from wells + half of fresh RPMI/B27-insulin) for 48 h until day 5. From day 5 to day 7, the cells were cultured in fresh RPMI/B27-insulin. By day 7, cells were then maintained with RPMI/B27 + insulin (B27 Supplement plus insulin, Gibco) with medium change every other day until day 15. Then, cells were collected for flow cytometry analysis to assess the purity of the differentiated hiPSC-CMs prior to cryopreservation. After differentiation, hiPSC-CMs with purity more than 70 % (% of cTnT$^+$ cells) were thawed and plated on 6-well plates coated with Synthemax (Corning) in EB20 media [20]. Once hiPSC-CMs attached within 2 days, the cells were cultured with RPMI/B27 + insulin (Gibco) for the next 7 days until contraction resumed. Following this period, the hiPSC-CMs were detached with TrypLE 10X (Gibco) and subsequently seeded onto the ECM scaffold for another 7 days to undergo further characterizations.

hiPSC-CF cell sheet fabrication

Anisotropic PDMS substrates were prepared from a silicon wafer master mold, with the grating dimensions of 5 μm depth, 15 μm width and 30 μm pitch, using SLYGARD 184 Silicone Elastomer Kit (Dow Corning, Midland, MI, USA) and cured at 65 °C for 4 h. Isotropic PDMS was casted from a flat plastic petri dish. Prior to cell culture, anisotropic or isotropic PDMS substrates were coated with polydopamine and collagen I as previously described [21]. In brief, 0.01 % W/V of 3-hydroxytyramine hydrochloride (Dopamine-HCl) (ACROS Organics, Fisher scientific, Hampton, NH, USA) was poured onto PDMS substrates for 24 h immersion. Followed by sterilization with ethylene oxide gas, polydopamine-coated PDMS was then second coated with bovine collagen (20 μg/ml) (Sigma Aldrich, St. Louis, MO, USA) for 2 h, then rinsed once with FibroGro Complete Media Kit (Millipore, replaced Glutamine with the equal amount of GlutaMAX (Thermo Scientific)), supplemented with 20 % fetal bovine serum (FBS, R&D systems, Minneapolis, MN, USA). hiPSC-CFs cultured in FibroGro Complete Media Kit + 20 % FBS were then seeded onto micropatterned PDMS at a density of 10,000 cells/cm^2 for up to 10 weeks. The medium was changed every other day until the desired time point was reached (2, 4, 6, 8, or 10 weeks).

hiPSC-CF cell sheet decellularization

Two decellularization solutions (A and B) were prepared: Solution A contained 1 M NaCl, 10 mM Tris (Bio-Rad, Hercules, CA, USA), and 5 mM EDTA (Sigma), while Solution B consisted of 0.1 % SDS (Sigma), 10

mM Tris, and 25 mM EDTA. hiPSC-CF cell sheets were first immersed into Solution A and gently agitated on slow shaker at room temperature (RT) for 1 h. Followed by three phosphate buffered saline (PBS) washes, cell sheets were then incubated in Solution B with gentle agitation at RT for 30 min. After three PBS washes, cell sheets were incubated in Dulbecco's Modified Eagle Medium (DMEM, Fisher Scientific) supplemented with 20 % FBS for 48 h at RT. After incubation, decellularized ECM was washed with PBS twice prior to cryopreservation.

Immunofluorescence staining of ECM scaffold and hiPSC-CM

Prior to staining, hiPSC-CF-ECM (24-well size, diameter of 14 mm) was fixed with 4 % paraformaldehyde (Fisher Scientific) and blocked with 1 % bovine serum albumin (BSA, Sigma-Aldrich) solution supplemented with 0.2 % Triton X-100 (Fisher Scientific), each for 30 min at RT. Immunofluorescence staining was performed to label specific ECM components on ECM scaffold. Primary antibodies targeting collagen I and fibronectin (1:200 in blocking solution, Abcam, Cambridge, MA, USA) were added to samples and incubate overnight at 4 °C. Samples were then washed three times with blocking solution. Secondary antibodies goat-anti mouse Alexa Fluor™ 488 conjugated or Alexa Fluor™ 594 conjugated (Invitrogen, Fisher Scientific) were added to samples and incubate for 1 h at RT. Cell nuclei were counterstained using 4′,6-diamidino-2-phenylindole (DAPI, Sigma). The specific ECM components and thickness was visualized and measured with confocal microscopy (Olympus FV-1000, Tokyo, Japan) and Olympus FLUOVIEW software.

Immunofluorescence staining of hiPSC-CM was conducted to label structural and functional proteins specific to native cardiomyocytes. After culturing hiPSC-CM on hiPSC-CF-ECM for 7 days, hiPSC-CM was fixed and blocked using the same solutions and conditions as described above. Primary antibodies targeting gap junction protein connexin 43 (Cx43, 1:200, Cell Signaling Technology), sarcomeric alpha-actinin (SAA, 1:200, Abcam), cardiac troponin T (cTnT, 1:200 Fisher Scientific), and F-actin (Phalloidin, 1:200, Cell Signaling Technology) were added to samples and incubate overnight at 4 °C. Samples were then washed three times with blocking solution and were stained with secondary antibodies goat-anti mouse Alexa Fluor™ 488 conjugated or Alexa Fluor™ 594 conjugated (Invitrogen, Fisher Scientific) for 1 h at RT. Cell nuclei were counterstained using 4′,6- diamidino-2-phenylindole (DAPI, Sigma). hiPSC-CMs were imaged with the confocal microscope (Leica SP8) and were analyzed with Leica LAS-X software. Sarcomere length of hiPSC-CMs was obtained by measuring two consecutive signals with clear striations in SAA staining and analyzed with ImageJ software.

DNA quantification

DNA assay was performed to compare hiPSC-CF proliferation following our previous protocol [22]. At intervals of 2, 4, 6, 8, 10 weeks of culture, cells were harvested and lysed using proteinase K solution (Sigma) at 37 °C overnight. The DNA content in the samples was determined using Quant-iT™ PicoGreen™ dsDNA Assay Kits (Fisher Scientific). In brief, 100 μL of lysed samples from each group and a DNA standard were placed in a 96-well plate. This was followed by mixing with 100 μL of Picogreen working solution and incubating for 10 min at RT. The incubated plate was then analyzed by microplate reader (Cytation 5, Biotek, Winooski, VT, USA) with excitation at 420 nm and emission at 520 nm wavelengths.

Quantification of ECM macromolecules

Commercially available assay kits were used to quantify the major ECM macromolecules in hiPSC-CF-ECM scaffold (24-well size, diameter of 14 mm), including fibronectin, total collagen, elastin, and sulfated glycosaminoglycan (sGAG). Fibronectin was quantified using an enzyme-linked immunosorbent assay (ELISA) following manufacturer's instruction (R&D Systems, Minneapolis, MN). Total collagen (soluble and insoluble) was measured by Sircol Assay (Biocolor Ltd., Carrickfergus, United Kingdom). Soluble collagen was extracted from ECM scaffold with 0.5 M acetic acid, whereas the insoluble residues underwent treatment with fragmentation reagent. Total collagen was then quantified following the manufacturer's protocol. The sGAG content was assessed using the Blyscan Sulfated Glycosaminoglycan Assay Kit (Biocolor Ltd.). After digestion with papain at 65 °C for 3 h and subsequent centrifugation at 10,000 x g for 10 min, the resulting supernatant was assayed according to the manufacturer's instructions. Elastin content was measured with Fasting Elastin Assay Kit (Biocolor Ltd.). Following treatment with 0.25 M oxalic acid at 100 °C for 1 h to convert insoluble elastin to water soluble α-elastin, the supernatant was collected upon centrifugation at 13,000 x g for 10 min, and then assayed according to the manufacturer's protocol. Absorbance measurements were read with a microplate reader (Cytation 5, Biotek) and were then utilized for the calculation of protein concentration.

Quantification of protein yield

Pierce™ bicinchoninic acid (BCA) assay kit (Thermo Scientific) was used to quantify the total protein yield in hiPSC-CF-ECM scaffold (24-well size, diameter of 14 mm). Samples were prepared in radioimmunoprecipitation (RIPA, Thermo Scientific) buffer with Halt™ Phosphatase Inhibitor Cocktail (Thermo Scientific) following the manufacturer's protocol. Samples were then sonicated using a sonic dismembrator (Fisher Scientific) for 2 s twice with a 5-seconds pause between at 80 % amplitude, then store on ice until testing. BCA assay was performed on each sample according to the manufacturer's instructions. Absorbance measurements were read with a microplate reader (Cytation 5, Biotek) and then utilized for the calculation of protein yield, production rate, and density.

Tensile testing

Young's modulus of the 6-week hiPSC-CF-ECM was determined through elongation tensile testing. Rectangular ECM sheets with dimensions 60 mm x 60 mm x 20 μm (length x width x thickness) were prepared. Rectangular sheet was then cut and folded into specimens measuring 15 mm x 30 mm x 40 μm (length x width x thickness) for each testing. Each specimen was soaked in PBS for 15 min prior to testing. The tensile testing was performed using Instron 5944 Universal Testing System (Instron Test Systems, Norwood, MA, USA) equipped with tensile clamps. Specimens were strained at a rate of 1 mm/min. Young's modulus (E) was calculated from the resulting stress–strain curves using equation: $E = \sigma/\varepsilon$, where σ denotes the uniaxial force per unit area, and ε is the strain or the proportional deformation.

Liquid chromatography-mass spectrometry (LC-MS)-based compositional evaluation

LC-MS-based compositional analysis of ECM scaffold was performed by Creative Proteomics (Shirley, NY, USA). 6-week hiPSC-CF-ECM were digested by trypsin, identified and quantified by applying nano LC-MS/MS platform comprising Ultimate 3000 nano UHPLC system coupled with a Q Exactive HF mass spectrometer (Thermo Scientific) with an ESI nanospray source. Detailed methods with sample preparation, nano LC-MS/MS Analysis and data analysis are provided in the Supplementary methods.

hiPSC-CM beating analysis

The beating rate and maximum principal strain variation were calculated from time-lapse videos using Digital Image Correlation (DIC) in the DaVis software (DaVis 10.2.1, LaVison, Gottingen, Germany). DIC tracks the in-plane mechanical deformation by partitioning each image

into smaller areas (subsets), and the movement of each subset is individually traced between consecutive images collected over time. The maximum principal mechanical strain within each subset, which stands for the material elongation during contraction cycles, is calculated by taking a partial derivative of the deformation field. In this study, time-lapse videos comprising approximately 300 images (frame size 704 μm × 532 μm) were analyzed with a subset size of ~ 94 μm and a step size of 3.5 μm. From each video, regions of interest (ROIs) with high cell density were pinpointed and selected for additional examination. The beating rate is determined from the number of periodic variations in maximum principal strain in the ROIs within a specific time duration.

Statistical analysis

Statistical comparisons among experimental groups were conducted through ordinary one-way ANOVA and Tukey's post hoc test using GraphPad Prism 10 software (GraphPad Software, Boston, MA, USA). All experiments were performed with biological triplicates, each consisting of at least four technical replicates. Image-based analysis involved capturing six non-overlapping images from each biological replicate ($N = 3$) within every experimental group. The details of experimental replicates are provided in the figure legends. Results are displayed as mean ± standard deviation (SD). Statistical significance was determined for $^{*}p < 0.05$, $^{**}p < 0.01$, $^{***}p < 0.001$, $^{****}p < 0.0001$, and nonsignificant (ns) for $p > 0.05$.

Results

hiPSC-CF-ECM characterization

Cardiac-specific ECM were obtained by culturing hiPSC-CFs on micro-grated PDMS for up to 10 weeks, followed by decellularization. Immunofluorescence staining showed highly aligned architecture of collagen I and fibronectin in both cell sheets and ECM (Fig. 1A, S1). Quantification of DNA concentration in cell sheets demonstrated a significant increase in cell proliferation after 6 weeks of culture (19.8 ± 0.6 μg/scaffold) compared with the 2-week (8.5 ± 2.4 μg/scaffold) and 4-week (15.0 ± 1.6 μg/scaffold) cultures, while no significant change was shown with 8-week cell sheets, but a significantly decrease with 10-week cultured cell sheets (14.0 ± 1.3 μg/scaffold) (Fig. 1B). Following decellularization, no DAPI signal was detected (Fig. 1A), and the efficacy of cell removal was quantified by measuring DNA concentration of hiPSC-CF-ECM cultured after 6 weeks. The DNA residual of hiPSC-CF-ECM after decellularization was less than 50 ng/mg ECM dry weight (7.8 ± 2.5 ng/mg) (Fig. 1C).

After 6 weeks of culture, collagen I thickness showed a significant increase (20.0 ± 2.1 μm) compared with the 2-week (12.3 ± 1.2 μm) and 4-week (15.0 ± 2.0 μm) cultures. However, no significant change was shown after culturing for 8 weeks and 10 weeks (Fig. 1D, 1F). Similarly, fibronectin thickness at 6-week also showed significantly higher thickness (19.8 ± 1.2 μm) than the 2-week (14.4 ± 1.8 μm) and 4-week ECM (14.6 ± 1.7 μm), while no significant change was observed after culturing for 8 weeks and 10 weeks (Fig. 1E, 1F). The protein amount of hiPSC-CF-ECM was also quantified using the BCA assay to measure the total protein yield, which displayed a trend similar to the thickness results (Fig. 1D, E), with an increase from week 2 to week 6 followed by a plateau (Fig. S2A). These results suggested that increase accumulation of ECM is associated with increase cell proliferation. To assess the long-term culture impact on ECM composition, major ECM macromolecules in hiPSC-CF-ECM cultured for 6, 8, 10 weeks were quantified, including collagen, fibronectin, elastin and sGAGs. The results indicated no significant differences in the amount of major ECM macromolecules among the three time points (Fig. 1G-J).

Compositional evaluation of hiPSC-CF-ECM.

Given no significant differences in ECM thickness and macromolecules across different culture times, the hiPSC-CF-ECM cultured for 6 weeks was selected as the optimal ECM scaffold for further analysis. Accordingly, a comprehensive compositional evaluation of the 6-week hiPSC-CF-ECM were analyzed. Nearly 1,300 peptides were identified in the ECM scaffold and the protein abundance was determined based on the LFQ intensities (Supplementary Excel Sheet). The pie graph depicted the 20 most abundant proteins among all detected peptides in the scaffold, with the sum of the remaining peptides labeled as "other" (Fig. 2A). The composition of 6-week hiPSC-CF-ECM indicated that fibronectin was the most abundant component in the ECM scaffold. Moreover, ECM scaffold was analyzed for the expression of native cardiac-specific fibrillar collagens (Fig. 2B), non-fibrillar collagens (Fig. 2C), and matricellular proteins (Fig. 2D). This compositional analysis revealed the presence of diverse fibrillar and non-fibrillar collagens that were abundant in the 6-week hiPSC-CF-ECM.

Tensile testing of hiPSC-CF-ECM

The tensile strength of the 6-week hiPSC-CF-ECM was analyzed by stretching along and across the aligned/anisotropic pattern, and compared with random/isotropic ECM under wet state (Fig. 3A-B). Stress–strain curve was used to calculate the young's modulus, maximum stress, and toughness (Fig. 3C). Among all groups, stretching along-fibers of the ECM showed highest modulus (E = 1.0 ± 0.27 MPa), maximum stress (430.3 ± 111.5 kPa), and toughness (268.6 ± 184.7 kJ/m^3) compared with stretching across-fiber in aligned pattern and random-fibers in isotropic pattern (Fig. 3D-F). These results suggested that 6-week hiPSC-CF-ECM is mechanically strong due to its sufficient thickness and anisotropic organization.

hiPSC-CMs on hiPSC-CF-ECM scaffold

In order to assess the capability of ECM scaffolds in fostering *in vitro* cell culture, hiPSC-CMs were grown on the 6-week hiPSC-CF-ECM for 7 days, followed by evaluation of cell morphology (Fig. 4). hiPSC-CMs cultured on the hiPSC-CF-ECM arranged into a condensed and highly oriented cellular assembly, aligning with the anisotropic orientation of ECM nanofibers (Fig. S3), which resembles the structure of native heart tissue. The cells also showed matured expression and organization of key structural proteins, including SAA and F-actin, suggesting native-like sarcomere structure. Moreover, hiPSC-CMs exhibited matured expression of functional proteins specific to native cardiomyocytes, such as cTnT and gap junction protein Cx43.

Contractile properties of hiPSC-CMs on hiPSC-CF-ECM

To evaluate the contractility functions, videos of beating hiPSC-CMs were taken after 7 days of culture on 6-week hiPSC-CF-ECM scaffold. Displacement vectors between reference and deformed frames were identified across various fields of view, and maximum principal strain values in the cardiomyocytes were calculated from the vectors. DIC-based analysis revealed that hiPSC-CMs cultured on the 6-week ECM scaffold exhibited a maximum principal strain variation of 0.009 ± 0.005 throughout the beating cycle. The beating rate, measured by the number of periodic maximum principal strain variation cycles during a fixed time period, was determined to be 3.39 ± 0.15 s per beat. Sarcomere length of hiPSC-CMs, measured via two consecutive signals obtained from immunofluorescence staining of SAA (Fig. 5A), showed a length of 1.8 ± 0.3 μm in the 6-week hiPSC-CF-ECM. These findings provided insights into the contractile capacity of hiPSC-CMs on ECM scaffolds (Fig. 5B).

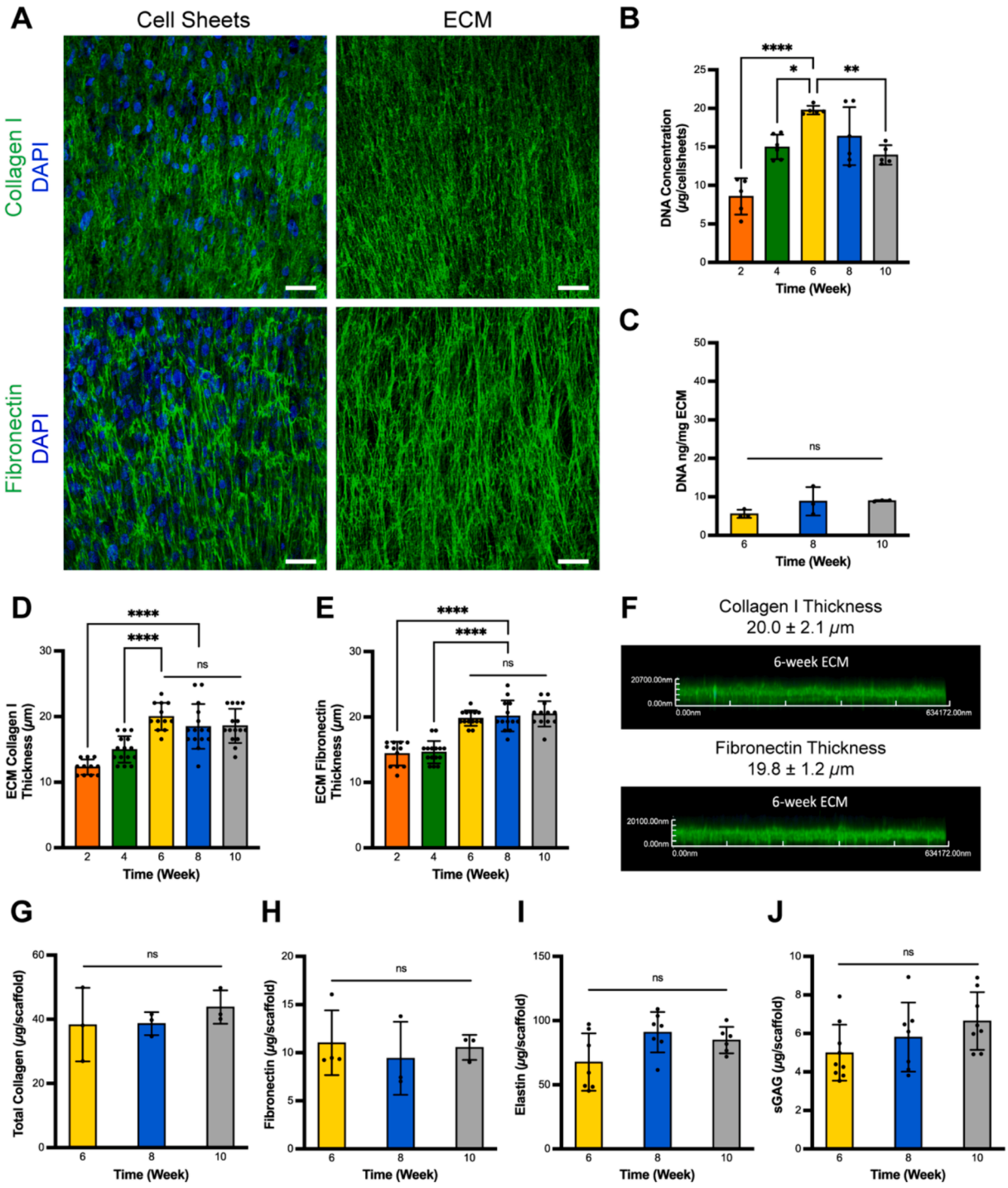

Fig. 1. Morphology, thickness, DNA content and ECM macromolecules of hiPSC-CF-ECM (A) Immunofluorescence images of hiPSC-CF sheets and ECM reveal anisotropic organization of key ECM proteins, collagen I (green), fibronectin (green), and cell nuclei via DAPI (blue). Scale bar: 50 μm. **(B)** Quantification of DNA concentration in hiPSC-CF sheets to estimate cell proliferation. Mean values are calculated from at least five technical replicates, based on three biological replicates. Error bar, SD. *$p < 0.05$, **$p < 0.01$, ****$p < 0.0001$ by ordinary one-way ANOVA. **(C)** Quantification of DNA concentration in hiPSC-CF-ECM to determine decellularization efficacy. Mean values are calculated based on three biological replicates. Error bar, SD. ns: $p > 0.05$ by ordinary one-way ANOVA. Comparison of hiPSC-CF-ECM thickness at various culture duration via **(D)** collagen I and **(E)** fibronectin staining. Mean values are calculated from at least ten technical replicates, based on three biological replicates. Error bar, SD. ****$p < 0.0001$ and ns: $p > 0.05$ by ordinary one-way ANOVA. **(F)** Representative Z-stack confocal images showing measurement of hiPSC-CF-ECM thickness. Quantification of **(G)** total collagen, **(H)** fibronectin, **(I)** elastin, and **(J)** sGAGs in hiPSC-CF-ECM scaffold after 6, 8, 10 weeks of culture. Mean values are calculated from at least three technical replicates, based on three biological replicates. Error bar, SD. ns: $p > 0.05$ by ordinary one-way ANOVA. (For interpretation of the references to colour in this figure legend, the reader is referred to the web version of this article.)

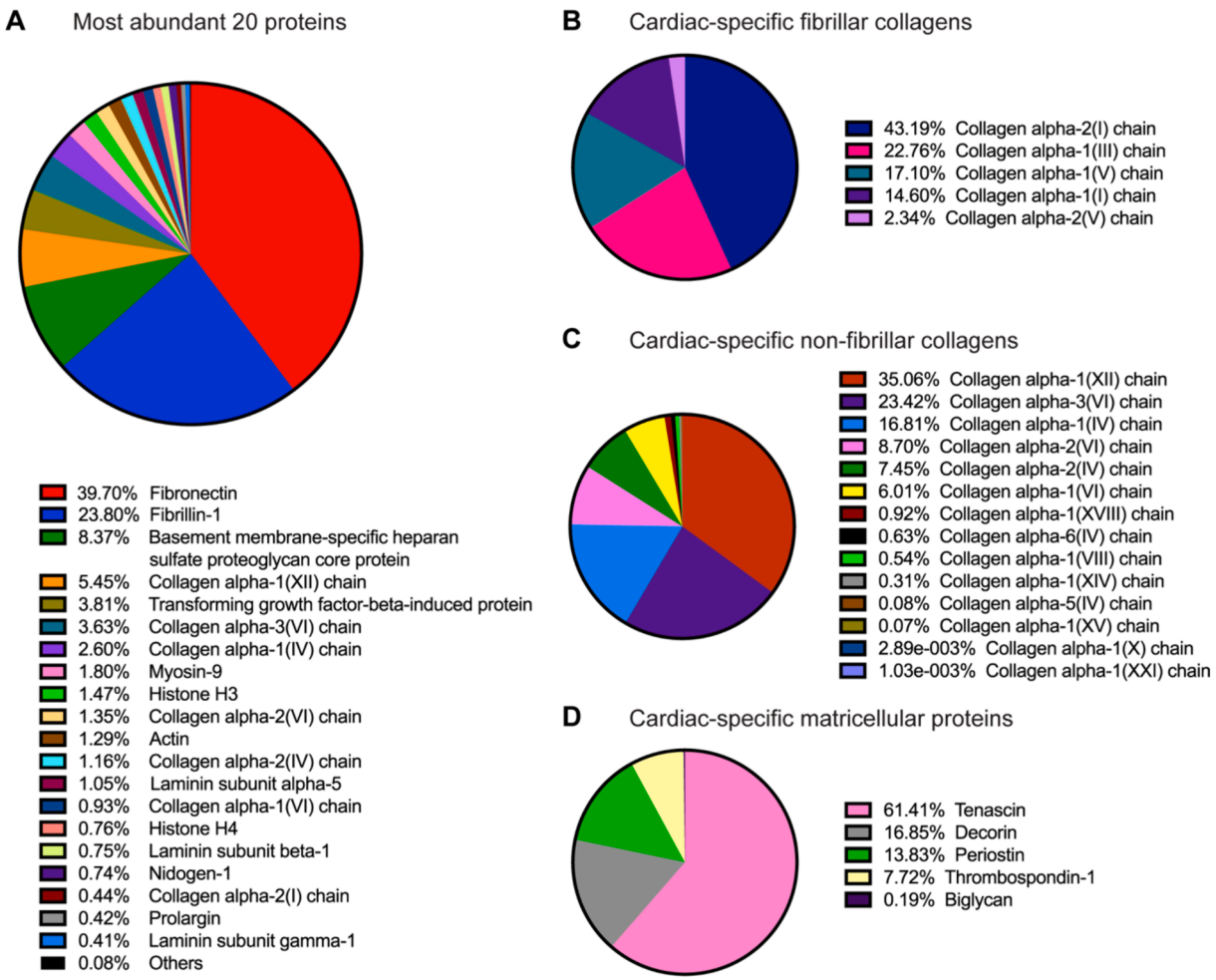

Fig. 2. Compositional evaluation of hiPSC-CF-ECM. Complete compositional evaluation of 6-week hiPSC-CF-ECM scaffolds via LC-MS including **(A)** most abundance 20 proteins depicted via pie chart based on LFQ intensities of each protein to indicate their abundance within scaffold. The abundance of cardiac-specific **(B)** fibrillar collagens, **(C)** non-fibrillar collagens, and **(D)** matricellular proteins using LFQ intensities from the LC-MS analysis. N = 3 biological replicates.

Discussion

In this study, hiPSC-CFs were cultured up to 10 weeks on micro-patterned substrate and subsequently decellularized to create aligned hiPSC-CF-ECM scaffold. Guided by contact guidance, hiPSC-CFs followed the micro-grated pattern in response to topography-driven alignment, where anisotropic surface pattern places lateral constraints on focal adhesions and actin stress fibers, facilitating force generation and directing specific cellular elongation and alignment [23]. Consequently, an anisotropic hiPSC-CF-ECM structure was well preserved even after the decellularization (Fig. 1A, S1). The anisotropic hiPSC-CF-ECM nanofibers that replicate the geometric cues of the myocardium facilitates the alignment of cardiomyocyte myofibrils (Fig. 4, S3), which could enhance structural integrity, increase contractile performance, and improved calcium metabolism [24,25].

One of the limitations of using cell-derived matrix is achieving sufficient *in vitro* production of ECM for scaffold fabrication within a short timeframe. In order to shorten the culture duration, previous studies have implemented various additives or supplements to enhance the ECM production. Macromolecular crowders such as Carrageenan, Ficoll or dextran, have been proposed to promote matrix deposition by creating confined spaces and restricting free diffusion to accelerate enzymatic processes [26–28]. Nevertheless, these macromolecular crowders interfere with cells and impede their alignment following underlying topographical cues [27,28]. Additionally, the unavoidable retention of crowding agent residuals after decellularization poses the risk of immune responses upon subsequent implantation [28]. These potential drawbacks could hinder the development of a biocompatible scaffold capable of accurately mimicking the native cardiac structure. On the other hand, ascorbic acid, which has been recognized for its ability to improve collagen production [29,30], was included in our culture medium. To examine whether the increased ascorbic acid concentration improves ECM fabrication, the thickness of ECM deposited from hiPSC-CFs cultured with different concentrations of ascorbic acid was measured. However, no significant difference was observed across the concentrations ranging from 50 to 200 μg/ml (Fig. S4). This implies that increasing ascorbic acid concentration may not be a viable strategy, possibly due to saturation of cellular uptake and regulated metabolism [31].

The ECM deposition is correlated with cell proliferation, as indicated by DNA quantification. The DNA content at the initial time points increased with culture time from 2 weeks to 6 weeks (Fig. 1B), corresponding to an increased ECM thickness (Fig. 1D-E). However, a decrease of DNA was observed after 6 weeks of culture (Fig. 1B), coinciding with the peak thickness of ECM deposition (Fig. 1D-F). This may be attributed to the insufficient nutrients diffusion to sustain layers of cell viability. Besides, when a higher cell seeding density was used to further increase cell quantity, a similar trend was also observed that the cell proliferation plateaued after 6 weeks (Fig. S5), and no difference in cell proliferation was observed between different seeding densities. These results suggested that extending the culture time represents a feasible approach for improved ECM deposition before reaching the

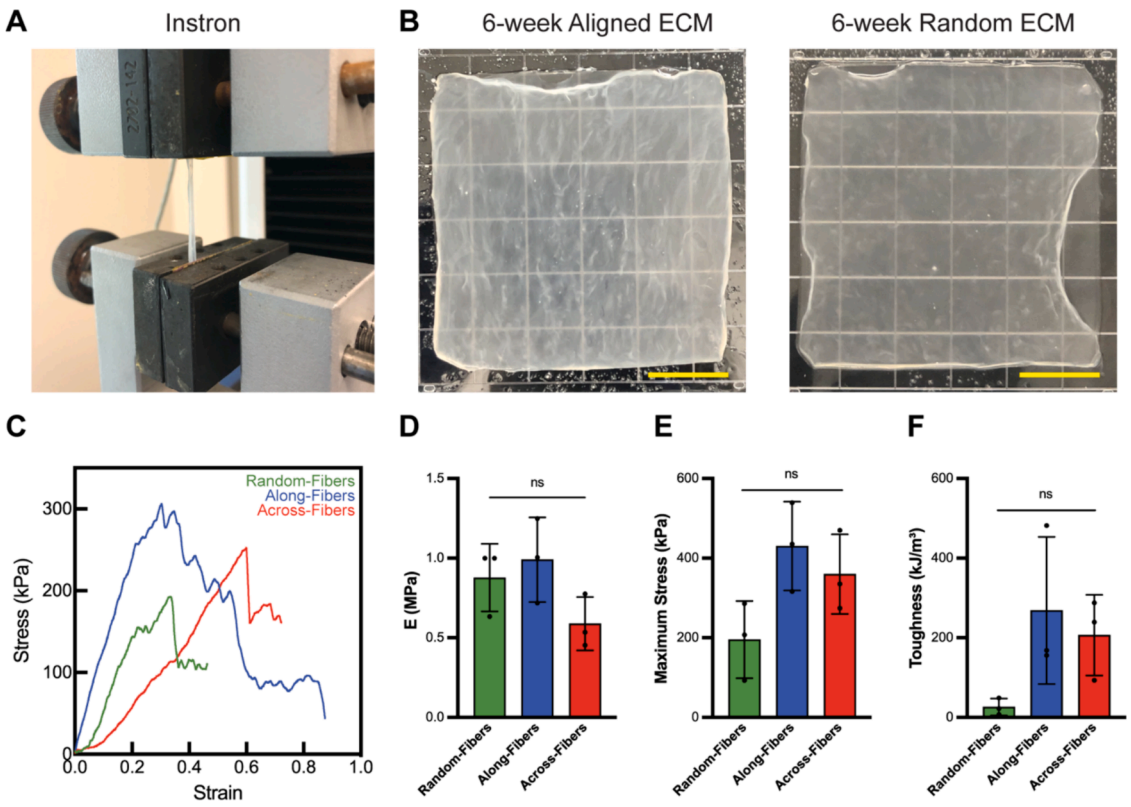

Fig. 3. Mechanical characterization by uniaxial tensile stretching of 6-week hiPSC-CF-ECM scaffold. **(A)** A setup for stretching hiPSC-CF-ECM using a tensile testing device. **(B)** Gross morphology of 6-week hiPSC-CF-ECM cultured on aligned vs. random pattern substrate. Scale bar: 2 cm. **(C)** Stress–strain curves of hiPSC-CF-ECM scaffolds oriented randomly, along the pattern and across the pattern. **(D)** Young's modulus, **(E)** maximum stress, and **(F)** toughness of ECM scaffolds quantified from the stress–strain curves. Mean values are calculated based on three biological replicates. Error bar, SD. ns: $p > 0.05$ by ordinary one-way ANOVA.

diffusion limit, while increasing cell seeding density appeared to be inefficient. Notably, DNA residual of hiPSC-CF-ECM after long-term culture was less than 50 ng/mg ECM dry weight (Fig. 1C), which has met the standard for DNA remnant in decellularized biomaterials after cell removal [32]. Furthermore, it is noteworthy that the ECM protein yield during week 2 to week 6 displayed a high linearity (Fig. S2B), corresponding to a production rate of 13.5 μg per day per 20,000 cells seeded. To further investigate the dynamic of ECM fabrication, we evaluated the "relative density" by dividing the protein yield of ECM by its volume (surface area × thickness; Fig. S2C). The ECM density increased from 2 to 6 weeks, indicating that protein secretion outpaced thickness growth. Overall, the dynamic quantifications reveal that our hiPSC-CF-ECM gradually becomes more compacted over the culture period.

The thickness of the decellularized ECM is a critical factor in cardiac patch engineering. While insufficient thickness compromises mechanical support during patch preparation and may increase susceptibility to tearing or damage during handling and implantation procedures, excessive thickness poses a barrier for effective cell infiltration into the matrix, hindering the integration of the native circulatory system. An overly thick construct often requires pre-assembled microvasculature to ensure adequate oxygen and nutrients perfusion for the survival of implanted cells [33,34]. In the native heart, the average intercapillary distance of microvasculature is 20 μm [35], which is close to the observed thickness in our hiPSC-CF-ECM (Fig. 1F). This biomimetic dimension suggests hiPSC-CF-ECM as a physiological relative tissue structure that would allow sufficient oxygen and nutrient diffusion, enhance cell viability, accelerate host integration, and promote angiogenesis.

To recreate the complexity of the myocardium, it is important to preserve the diverse proteomics in the scaffold. In the native adult cardiac ECM, fibrillar collagen is constitutes about 70 % of the total protein content. Basement membrane proteins (e.g. agrin, collagen IV, perlecan, laminin, and nidogen) represent about 20 % of the ECM, while matricellular proteins (e.g. collagen V-VI, fibronectin, periostin, fibulin, emilin, thrombospondin, and lumican) account for 3–5 %. The remaining 4 % comprises other structural protein, including proteoglycan and fibrous glycoproteins [36,37]. Our result showed that the major ECM macromolecules were successfully retained in the hiPSC-CF-ECM after decellularization (Fig. 1G-J), which only causes a moderate loss of protein (as shown in our previous study [18]). More importantly, cardiac ECM undergoes drastic physiological and pathological remodeling during development, where fetal or neonatal ECM contains abundance of fibronectin, fibrillin, collagen VI, and periostin that are replaced by collagen I, collagen III and laminin with age [38,39]. Such differences in ECM composition between fetal and adult stages are associated with declined cardiomyocyte proliferation during aging and are key to developing an approach for maturing cardiomyocytes [39,40]. Our LC-MS analysis demonstrated the high abundance of protein components enriched in native fetal cardiac ECM, including fibronectin (37.7 %), fibrillin (23.8 %), and collagen VI (~5.91 %) within the hiPSC-CF-ECM (Fig. 2A), which are crucial for maintaining the functionality of the ECM scaffold [14] and supporting hiPSC-CM culture (Fig. 5).

In addition to good morphological and compositional properties to support cardiomyocyte function, the optimal ECM scaffold should also recapitulate the mechanical properties of native myocardium for successful transplantation of cardiac patch. The anisotropic mechanical strength of healthy myocardium is given by its unique cellular and ECM nanoscale arrangement [41]. While the along-fibers group exhibited higher strength compared to across-fibers or random-fibers (Fig. 3), these differences did not reach statistical significance. This phenomenon

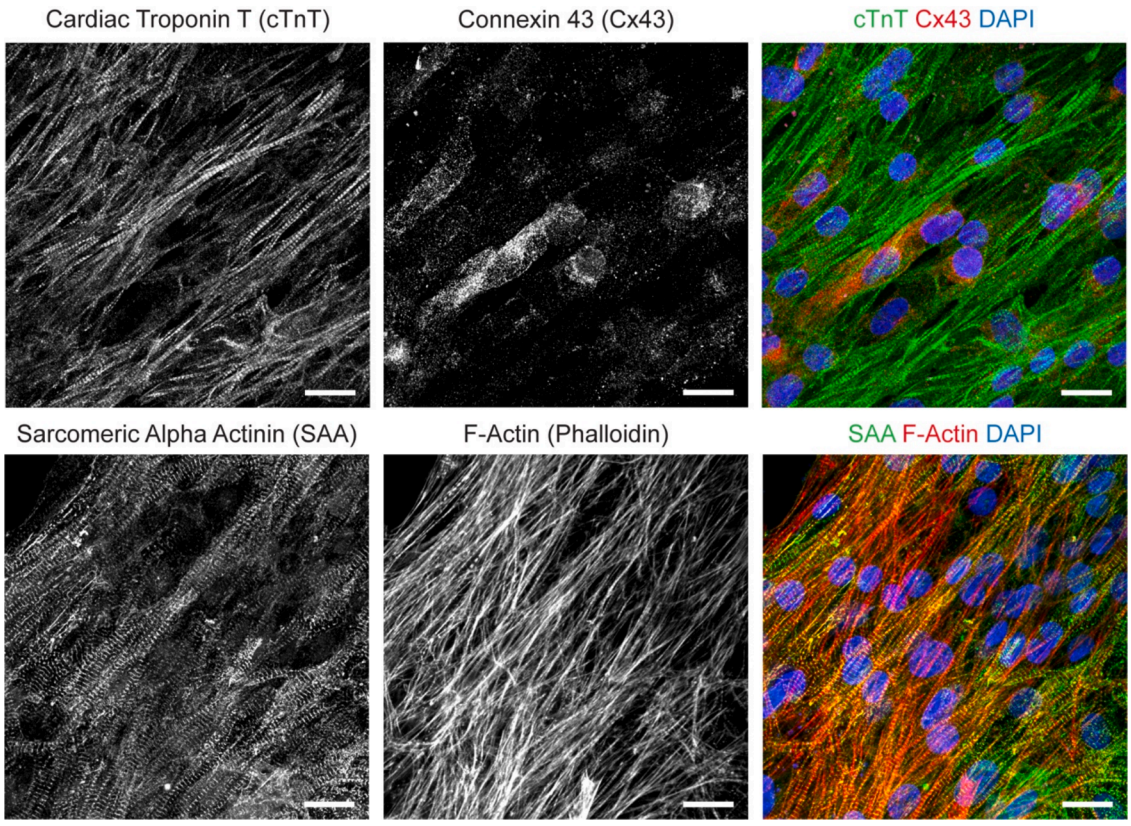

Fig. 4. Evaluation of native cardiomyocyte-specific structural and function protein organization in hiPSC-CMs cultured on hiPSC-CF-ECM. hiPSC-CMs cultured on 6-week hiPSC-CF-ECM were oriented in aligned direction following ECM fiber anisotropy. hiPSC-CMs showed mature organization of key structural and functional proteins including cTnT, Cx43, SAA, and F-actin. Scale bar 20 μm.

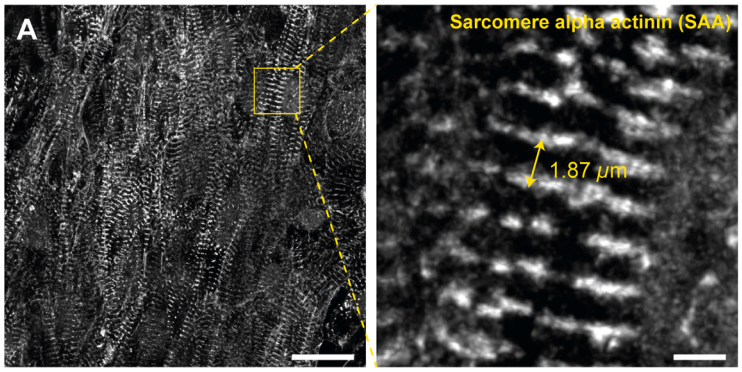

B

hiPSC-CMs on 6-week hiPSC-CF-ECM	
Maximum Principal Strain	0.009 ± 0.005
Beating Cycle (seconds/beat)	3.39 ± 0.15
Sarcomere Length (μm)	1.8 ± 0.3

Fig. 5. Evaluation of hiPSC-CMs contractile properties on 6-week hiPSC-CF-ECM scaffold. (A) Immunofluorescence staining-based sarcomere length measurement. hiPSC-CMs on 6-week hiPSC-CF-ECM were stained with SAA to measure the distance between the two consecutive signals. Scale bar: 20 μm (left) and 2 μm (right). **(B)** Maximum principal strain, beating cycle, and sarcomere length of hiPSC-CMs on 6-week hiPSC-CF-ECM. N = 3 biological replicates. Results displayed as mean ± SD.

is likely attributed to fiber organization. The quantification of collagen fiber alignment in the 6-week hiPSC-CF-ECM showed a peak at 89.25° representing clear alignment. Nevertheless, a dispersion of 17.34° exists (Fig. S1), suggesting that the 15 μm-wide micropattern grooves resulted in the formation of crossed nanofibers with a dispersion angle close to 15°. These crossed fibers provide the mechanical strength during across-fibers stretching, leading to non-significantly different tensile strengths in both directions. Furthermore, cardiac scaffold should be mechanical strong, that is about 0.5 MPa of Young's modulus reported in actively contracting human heart tissue [42], to bear constantly preload from blood filling the cavities during *in vivo* heart pulsation. Our hiPSC-CF-ECM showed slightly higher Young's modulus compared to the native tissue, which might be attributed to the effects of buoyancy, hydration or drying on the tissue during mechanical testing. Nevertheless, the measured stiffness at the same scale as the literature value suggested sufficient mechanical strength for cardiac patch applications. Besides, the ECM fibers exhibited different rupture points during the stretching test, resulting in a large variation in toughness measurement. This observation indicated distinct load-bearing capacities among individual fibers, suggesting that the ECM undergoes continuous remodeling under tension.

To assess the effectiveness of hiPSC-CF-ECM in engineering cardiac patches, hiPSC-CMs were cultured on the anisotropic hiPSC-CF-ECM and showed improved phenotypic expression and maturation, including

cTnT, SAA, Cx43, and F-Actin (Fig. 4). The contraction of the heart is regulated by structural protein cTnT, which modulates the calcium-dependent interaction between actin and myosin [43]. SAA contributes to the contractile strength of cardiac muscle fiber by engaging in crosslinking with actin filaments, organizing the thin filaments into a repetitive pattern [44]. The gap junction protein Cx43 creates channels between neighboring cells, facilitating ion exchange and supporting synchronized heart contraction by propagating action potentials [45]. While we have observed Cx43 at membranes between cells, perinuclear labeling and cell surface expression of Cx43 are also present on hiPSC-CMs. Although the mechanism governing Cx43 localization and function within the nucleus remains unclear, it has been suggested that this expression may play roles in cardioprotection and in regulating cell growth and differentiation [46]. Additionally, there are speculations that changes in nuclear Cx43 levels alter the gene expression profile and pathological phenotype of the heart during development and disease [47]. The organization of structural and functional proteins present here suggests that hiPSC-CF-ECM has the potential to facilitate the maturation of hiPSC-CMs. Furthermore, highly aligned sarcomere structures were observed in hiPSC-CM culture (Fig. 5A), which are the fundamental contractile units of myofibrils in cardiomyocytes. The measured sarcomere length on the 6-week ECM closely resembled the length of native sarcomeres (1.8 μm) [48]. These results further confirmed that 6 weeks of culture is sufficient for hiPSC-CF-ECM fabrication as a cardiac patch scaffold.

Conclusion

This study aimed to achieve an appropriate ECM deposition, scaffold thickness and mechanical strength of a hiPSC-CF-ECM scaffold by optimizing the culture time of hiPSC-CFs. Results indicated that the after 6 weeks of culture, the ECM derived from hiPSC-CFs not only exhibits mechanically robustness but also incorporates essential cardiac-specific bioactive molecules. Furthermore, this ECM scaffold facilitated the matured organization of key cardiomyocyte-specific structural and functional proteins of hiPSC-CMs, indicating its promise for cardiac patch engineering.

CRediT authorship contribution statement

Te-An Chen: Writing – original draft, Visualization, Validation, Methodology, Investigation, Formal analysis, Data curation, Conceptualization. **Brandon B. Zhao:** Formal analysis, Data curation. **Richard A. Balbin:** Formal analysis, Data curation. **Sameeksha Sharma:** Formal analysis, Data curation. **Donggi Ha:** Writing – review & editing, Methodology, Formal analysis, Data curation. **Timothy J. Kamp:** Writing – review & editing, Resources, Funding acquisition. **Yuxiao Zhou:** Writing – review & editing, Validation, Methodology. **Feng Zhao:** Writing – review & editing, Validation, Supervision, Project administration, Funding acquisition, Conceptualization.

Declaration of competing interest

The authors declare that they have no known competing financial interests or personal relationships that could have appeared to influence the work reported in this paper.

Data availability

Data will be made available on request.

Acknowledgments

We acknowledge Texas A&M University Microscopy and Imaging Center Core Facility (RRID:SCR_022128) for providing microscopy resources. This study was funded by the National Institutes of Health (R01HL146652) and National Science Foundation (2106048) to F.Z.; NIH U01 HL134764 and NSF 1648035 to T.J.K.

Appendix A. Supplementary data

Supplementary data to this article can be found online at https://doi.org/10.1016/j.mbplus.2024.100151.

References

[1] A. Eltom, G. Zhong, A. Muhammad, Scaffold techniques and designs in tissue engineering functions and purposes: a review, Adv. Mater. Sci. Eng. 2019 (2019).
[2] M.I. Echeverria Molina, K.G. Malollari, K. Komvopoulos, Design challenges in polymeric scaffolds for tissue engineering, Front. Bioeng. Biotechnol. 9 (2021) 617141.
[3] V. Mastrullo, W. Cathery, E. Velliou, P. Madeddu, P. Campagnolo, Angiogenesis in tissue engineering: as nature intended? Front. Bioeng. Biotechnol. 8 (2020) 188.
[4] S. Hinderer, S.L. Layland, K. Schenke-Layland, ECM and ECM-like materials—Biomaterials for applications in regenerative medicine and cancer therapy, Adv. Drug Deliv. Rev. 97 (2016) 260–269.
[5] X. Zhang, X. Chen, H. Hong, R. Hu, J. Liu, C. Liu, Decellularized extracellular matrix scaffolds: Recent trends and emerging strategies in tissue engineering, Bioact. Mater. 10 (2022) 15–31.
[6] A.A. Golebiowska, J.T. Intravaia, V.M. Sathe, S.G. Kumbar, S.P. Nukavarapu, Decellularized extracellular matrix biomaterials for regenerative therapies: Advances, challenges and clinical prospects, Bioact. Mater. 32 (2024) 98–123.
[7] H. Kobayashi, S. Tohyama, H. Kanazawa, H. Ichimura, S. Chino, Y. Tanaka, Y. Suzuki, J. Zhao, N. Shiba, S. Kadota, Intracoronary transplantation of pluripotent stem cell-derived cardiomyocytes: Inefficient procedure for cardiac regeneration, J. Mol. Cell. Cardiol. 174 (2023) 77–87.
[8] C. Liu, D. Han, P. Liang, Y. Li, F. Cao, The current dilemma and breakthrough of stem cell therapy in ischemic heart disease, Front. Cell Dev. Biol. 9 (2021) 636136.
[9] J.A. Schaefer, P.A. Guzman, S.B. Riemenschneider, T.J. Kamp, R.T. Tranquillo, A cardiac patch from aligned microvessel and cardiomyocyte patches, J. Tissue Eng. Regen. Med. 12 (2) (2018) 546–556.
[10] I.Y. Shadrin, B.W. Allen, Y. Qian, C.P. Jackman, A.L. Carlson, M.E. Juhas, N. Bursac, Cardiopatch platform enables maturation and scale-up of human pluripotent stem cell-derived engineered heart tissues, Nat. Commun. 8 (1) (2017) 1825.
[11] X. Lou, Y. Tang, L. Ye, D. Pretorius, V.G. Fast, A.M. Kahn-Krell, J. Zhang, J. Zhang, A. Qiao, G. Qin, Cardiac muscle patches containing four types of cardiac cells derived from human pluripotent stem cells improve recovery from cardiac injury in mice, Cardiovasc. Res. 119 (4) (2023) 1062–1076.
[12] R.J. Jabbour, T.J. Owen, P. Pandey, M. Reinsch, B. Wang, O. King, L.S. Couch, D. Pantou, D.S. Pitcher, R.A. Chowdhury, In vivo grafting of large engineered heart tissue patches for cardiac repair, JCI Insight 6 (15) (2021).
[13] D. Sharma, M. Ferguson, F. Zhao, A step-by-step protocol for generating human fibroblast cell-derived completely biological extracellular matrix scaffolds, Methods Cell Biol. (2020) 3–13.
[14] A.C. Silva, C. Pereira, A.C.R. Fonseca, P. Pinto-do-Ó, D.S. Nascimento, Bearing my heart: the role of extracellular matrix on cardiac development, homeostasis, and injury response, Front. Cell Dev. Biol. 8 (2021) 621644.
[15] D. Fan, A. Takawale, J. Lee, Z. Kassiri, Cardiac fibroblasts, fibrosis and extracellular matrix remodeling in heart disease, Fibrogenesis Tissue Repair 5 (2012) 1–13.
[16] C. Bonnans, J. Chou, Z. Werb, Remodelling the extracellular matrix in development and disease, Nat. Rev. Mol. Cell Biol. 15 (12) (2014) 786–801.
[17] J. Zhang, R. Tao, K.F. Campbell, J.L. Carvalho, E.C. Ruiz, G.C. Kim, E.G. Schmuck, A.N. Raval, A.M. da Rocha, T.J. Herron, Functional cardiac fibroblasts derived from human pluripotent stem cells via second heart field progenitors, Nat. Commun. 10 (1) (2019) 2238.
[18] T.-A. Chen, D. Sharma, W. Jia, D. Ha, K. Man, J. Zhang, Y. Yang, Y. Zhou, T. J. Kamp, F. Zhao, Detergent-Based Decellularization for Anisotropic Cardiac-Specific Extracellular Matrix Scaffold Generation, Biomimetics 8 (7) (2023) 551.
[19] X. Lian, J. Zhang, S.M. Azarin, K. Zhu, L.B. Hazeltine, X. Bao, C. Hsiao, T.J. Kamp, S.P. Palecek, Directed cardiomyocyte differentiation from human pluripotent stem cells by modulating Wnt/β-catenin signaling under fully defined conditions, Nat. Protoc. 8 (1) (2013) 162–175.
[20] J. Zhang, G.F. Wilson, A.G. Soerens, C.H. Koonce, J. Yu, S.P. Palecek, J. A. Thomson, T.J. Kamp, Functional cardiomyocytes derived from human induced pluripotent stem cells, Circ. Res. 104 (4) (2009) e30–e41.
[21] D. Sharma, W. Jia, F. Long, S. Pati, Q. Chen, Y. Qyang, B. Lee, C.K. Choi, F. Zhao, Polydopamine and collagen coated micro-grated polydimethylsiloxane for human mesenchymal stem cell culture, Bioact. Mater. 4 (2019) 142–150.
[22] Z. Qian, D. Ross, W. Jia, Q. Xing, F. Zhao, Bioactive polydimethylsiloxane surface for optimal human mesenchymal stem cell sheet culture, Bioact. Mater. 3 (2) (2018) 167–173.
[23] C. Leclech, A.I. Barakat, Is there a universal mechanism of cell alignment in response to substrate topography? Cytoskeleton 78 (6) (2021) 284–292.
[24] T. Takada, D. Sasaki, K. Matsuura, K. Miura, S. Sakamoto, H. Goto, T. Ohya, T. Iida, J. Homma, T. Shimizu, Aligned human induced pluripotent stem cell-derived cardiac tissue improves contractile properties through promoting unidirectional and synchronous cardiomyocyte contraction, Biomaterials 281 (2022) 121351.

[25] C. Zhu, A.E. Rodda, V.X. Truong, Y. Shi, K. Zhou, J.M. Haynes, B. Wang, W. D. Cook, J.S. Forsythe, Increased cardiomyocyte alignment and intracellular calcium transients using micropatterned and drug-releasing poly (glycerol sebacate) elastomers, ACS Biomater Sci. Eng. 4 (7) (2018) 2494–2504.
[26] I.M. Kuznetsova, K.K. Turoverov, V.N. Uversky, What macromolecular crowding can do to a protein, Int. J. Mol. Sci. 15 (12) (2014) 23090–23140.
[27] M. Marinkovic, R. Sridharan, F. Santarella, A. Smith, J.A. Garlick, C.J. Kearney, Optimization of extracellular matrix production from human induced pluripotent stem cell-derived fibroblasts for scaffold fabrication for application in wound healing, J. Biomed. Mater. Res. A 109 (10) (2021) 1803–1811.
[28] S.W. Fok, R.C. Gresham, W. Ryan, B. Osipov, C. Bahney, J.K. Leach, Macromolecular crowding and decellularization method increase the growth factor binding potential of cell-secreted extracellular matrices, Front. Bioeng. Biotechnol. 11 (2023) 1091157.
[29] C. D'Aniello, F. Cermola, E.J. Patriarca, G. Minchiotti, Vitamin C in stem cell biology: impact on extracellular matrix homeostasis and epigenetics, Stem Cells Int. 2017 (2017).
[30] J. Kao, G. Huey, R. Kao, R. Stern, Ascorbic acid stimulates production of glycosaminoglycans in cultured fibroblasts, Exp. Mol. Pathol. 53 (1) (1990) 1–10.
[31] H. Qiao, J. Bell, S. Juliao, L. Li, J.M. May, Ascorbic acid uptake and regulation of type I collagen synthesis in cultured vascular smooth muscle cells, J. Vasc. Res. 46 (1) (2008) 15–24.
[32] P.M. Crapo, T.W. Gilbert, S.F. Badylak, An overview of tissue and whole organ decellularization processes, Biomaterials 32 (12) (2011) 3233–3243.
[33] T. Su, K. Huang, M.A. Daniele, M.T. Hensley, A.T. Young, J. Tang, T.A. Allen, A. C. Vandergriff, P.D. Erb, F.S. Ligler, Cardiac stem cell patch integrated with microengineered blood vessels promotes cardiomyocyte proliferation and neovascularization after acute myocardial infarction, ACS Appl. Mater. Interfaces 10 (39) (2018) 33088–33096.
[34] L. Wang, J. Zhang, Layer-by-layer fabrication of thicker and larger human cardiac muscle patches for cardiac repair in mice, Front. Cardiovasc. Med. 8 (2022) 800667.
[35] M.A. Biederman-Thorson, R.F. Schmidt, G. Thews, Human Physiology, Springer Science & Business Media, 2013.
[36] T.D. Johnson, R.C. Hill, M. Dzieciatkowska, V. Nigam, A. Behfar, K.L. Christman, K. C. Hansen, Quantification of decellularized human myocardial matrix: a comparison of six patients, Proteomics–clinical Applications 10 (1) (2016) 75–83.
[37] D. Bejleri, M.E. Davis, Decellularized extracellular matrix materials for cardiac repair and regeneration, Adv. Healthc. Mater. 8 (5) (2019) 1801217.
[38] S.G. Ozcebe, G. Bahcecioglu, X.S. Yue, P. Zorlutuna, Effect of cellular and ECM aging on human iPSC-derived cardiomyocyte performance, maturity and senescence, Biomaterials 268 (2021) 120554.
[39] C. Williams, K.P. Quinn, I. Georgakoudi, L.D. Black III, Young developmental age cardiac extracellular matrix promotes the expansion of neonatal cardiomyocytes in vitro, Acta Biomater. 10 (1) (2014) 194–204.
[40] H. Esmaeili, C. Li, X. Fu, J.P. Jung, Engineering extracellular matrix proteins to enhance cardiac regeneration after myocardial infarction, Front. Bioeng. Biotechnol. 8 (2021) 611936.
[41] A.W. Feinberg, P.W. Alford, H. Jin, C.M. Ripplinger, A.A. Werdich, S.P. Sheehy, A. Grosberg, K.K. Parker, Controlling the contractile strength of engineered cardiac muscle by hierarchal tissue architecture, Biomaterials 33 (23) (2012) 5732–5741.
[42] C. Bouten, P. Dankers, A. Driessen-Mol, S. Pedron, A. Brizard, F. Baaijens, Substrates for cardiovascular tissue engineering, Adv. Drug Deliv. Rev. 63 (4–5) (2011) 221–241.
[43] S. Sharma, P. Jackson, J. Makan, Cardiac troponins, BMJ Publishing Group (2004) 1025–1026.
[44] C.P. Hsu, B. Moghadaszadeh, J.H. Hartwig, A.H. Beggs, Sarcomeric and nonmuscle α-actinin isoforms exhibit differential dynamics at skeletal muscle Z-lines, Cytoskeleton 75 (5) (2018) 213–228.
[45] P. Beauchamp, K.A. Yamada, A.J. Baertschi, K. Green, E.M. Kanter, J.E. Saffitz, A. G. Kléber, Relative contributions of connexins 40 and 43 to atrial impulse propagation in synthetic strands of neonatal and fetal murine cardiomyocytes, Circ. Res. 99 (11) (2006) 1216–1224.
[46] A. Rodríguez-Sinovas, J.A. Sánchez, L. Valls-Lacalle, M. Consegal, I. Ferreira-González, Connexins in the heart: regulation, function and involvement in cardiac disease, Int. J. Mol. Sci. 22 (9) (2021) 4413.
[47] T. Martins-Marques, K. Witschas, I. Ribeiro, M. Zuzarte, S. Catarino, T. Ribeiro-Rodrigues, F. Caramelo, T. Aasen, I.M. Carreira, L. Goncalves, Cx43 can form functional channels at the nuclear envelope and modulate gene expression in cardiac cells, Open Biol. 13 (11) (2023) 230258.
[48] L. Burbaum, J. Schneider, S. Scholze, R.T. Böttcher, W. Baumeister, P. Schwille, J. M. Plitzko, M. Jasnin, Molecular-scale visualization of sarcomere contraction within native cardiomyocytes, Nat. Commun. 12 (1) (2021) 4086.